200 Gbit/s Barium Titanate Modulator Using Weakly Guided Plasmonic Modes

Daniel Chelladurai[1], Manuel Kohli[1], Bertold Ian Bitachon[1], Laurenz Kulmer[1], Tobias Blatter[1], David Moor[1], Joel Winiger[1], Andreas Messner[1], Clarissa Convertino[2], Felix Eltes[2], Yuriy Fedoryshyn[1] and Juerg Leuthold[1]

[1]Institute of Electromagnetic Fields (IEF), ETH Zurich, Gloriastrasse 35, 8092 Zurich, Switzerland
[2]Lumiphase AG, 8802 Kilchberg, Switzerland
Author e-mail address: daniel.chelladurai@ief.ee.ethz.ch, JuergLeuthold@ethz.ch

Abstract: A plasmonic Mach-Zehnder modulator based on thin-film barium titanate is introduced demonstrating line rates up to 200 Gbit/s. The structure enables low insertion loss and high optical power stability without a DC bias during operation. © 2022 The Author(s)

1. Introduction

Electro-optic modulators are a key component in photonic integrated circuits for optical communication systems. They encode electrical data onto optical signals and are required to do so at increasingly higher speeds to keep pace with global data usage trends [1, 2]. The next generation modulators should be able to transmit symbol rates reaching hundreds of GBaud with a small footprint to enable co-integrated electronics and low optical and electrical power consumptions [1, 3].

The fastest symbol rates are currently achieved with plasmonic-organic hybrid (POH) modulators where using the electrodes for waveguiding leads to ultra-high bandwidths that allow symbol rates exceeding 200 GBaud [4]. Their small footprints are enabled by organic electro-optic materials with large Pockels coefficients. Modulators based on the thin-film lithium niobate platform offer the lowest losses with excellent temperature and power stability. Recent demonstrations have shown dual-polarization IQ modulators operated at symbol rates of 130 GBaud [5]. The smaller Pockels coefficient of lithium niobate compared to organic materials, however, results in long device lengths of a few centimeters which increases the difficulty for electronic cointegration. Barium titanate (BTO) has emerged as a promising inorganic material with a large Pockels coefficient [6]. High symbol rates have been achieved in plasmonic modulators with a small footprint, though they use a DC bias during operation and the high intrinsic optical losses in plasmonic modulators leave room for improvement in optical power consumption [7, 8].

In this work we present a weakly guided plasmonic Mach-Zehnder modulator (MZM) structure that combines the plasmonic advantage of using the electrodes as the waveguides with the photonic advantage of lower insertion losses. The modulator uses BTO as the active material which allows the modulator to be only 500 µm in length with an on-chip insertion loss of 8 dB while being able to handle high optical powers of 20 dBm with no degradation over 12 hours of continuous operation. The efficient weakly guided plasmonic structure allows operation without a DC bias in contrast to typical BTO devices. We demonstrate intensity-modulation / direct-detection (IM/DD) data transmission with symbol rates of 128 GBaud for 2PAM and 100 GBaud for 4PAM with bit-error-ratios (BER) below the hard-decision forward error correction (HD-FEC) limit for PAM2 and soft-decision FEC (SD-FEC) for PAM4.

2. Modulator Design

Fig. 1(a) shows a cross-sectional schematic of a single arm of the weakly guided plasmonic MZM. The simple structure consists of a BTO layer on a buried oxide with gold electrodes placed on top and separated from the BTO by a thin oxide layer. The working principle of these weakly guided plasmonic waveguides is that the effective refractive index of the slab mode in the region between the metals is greater than that for the regions with metals, thus satisfying the requirements for waveguiding [9].

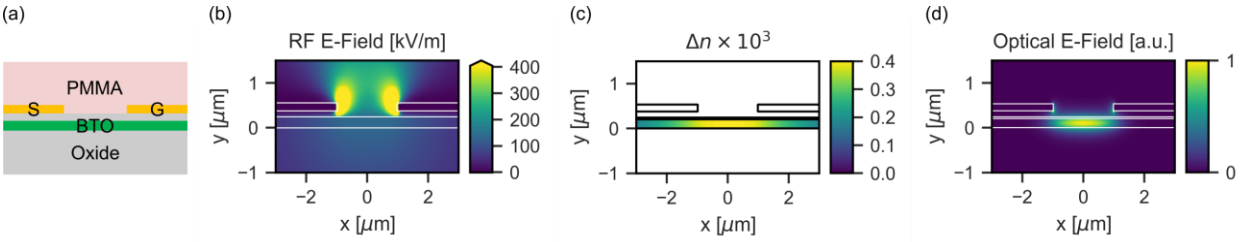

Fig. 1: (a) Cross-sectional schematic of the weakly guided plasmonic-photonic phase shifter. (b) RF electric field distribution (x-component) for a 1 V RF driving signal. (c) Change in refractive index of the BTO layer due to the RF electric field. (d) Optical mode profile.

Fig. 1(b) shows the RF electric field profile at 50 GHz calculated with FDTD simulations and assuming 1 V RF driving signal. The RF electric field distribution is used to calculate the spatially varying refractive index change in the BTO shown in Fig. 1(c). Even though the RF field does not perfectly overlap with the BTO layer, enough electric field is present to still achieve a large refractive index change. The optical mode profile is plotted in Fig. 1(d) with an arbitrary scale from 0 to 1. The waveguiding nature of the metals is clearly apparent and results in an optical mode that overlaps well with the region of the BTO that undergoes a refractive index change.

We simulate the dependence of the modulator's performance using FDTD simulations taking literature values for the clamped Pockels coefficients in BTO [10]. The dependence of the voltage-length product ($V_\pi L$) as well as the voltage-length-loss product ($V_\pi L\alpha$) on the electrode gap is shown in Fig. 2. The $V_\pi L$ (solid line) decreases with the gap size because the electric fields are larger for a given driving voltage. Optical propagation losses, however, increase dramatically for small electrode gaps, see Fig. 2(b), which leads to increasing $V_\pi L\alpha$, see Fig. 2(a) dashed line. This results in a tradeoff between the modulator's footprint and insertion loss. For a given V_π, a short device with a small electrode gap will have a larger insertion loss than a longer device with a wider electrode gap.

The conversion loss between access waveguides and phase shifters follows a similar trend as shown in Fig. 2(c). Wider gaps have near lossless (0.05 dB) conversion into and out of the phase shifter while the smaller gaps have a small but non-negligible conversion loss (0.3 dB). We chose an electrode gap of 2 µm to keep the modulator length below 1 mm while maintaining a total device insertion loss below 10 dB. This represents a significant improvement over nm-scale plasmonic slot waveguides in BTO where mode conversion and propagation losses make it difficult to achieve insertion losses below 10 dB.

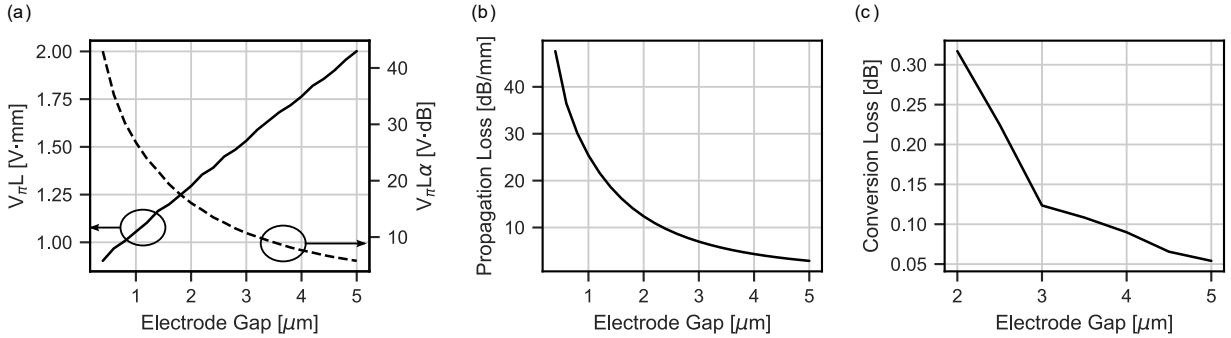

Fig. 2: Simulated phase-shifter characteristics for various distances between electrodes. (a) Voltage-length product (solid line) and voltage-length-loss product (dashed line) (b) Optical propagation loss. (c) Conversion loss between access waveguides and the phase-shifter.

The simple structure of the weakly guided plasmonic phase shifter begets a simple fabrication process as well. Starting with a BTO-on-insulator substrate, the first step is waveguide and grating coupler patterning using electron beam lithography (EBL) and subsequent dry etching. Next, the sample is annealed to reduce optical propagation losses [11]. After annealing, a thin oxide layer is deposited with PECVD. The electrodes are patterned with EBL and deposited with electron beam evaporation followed by lift off process. Finally, the sample is covered with a PMMA cladding. The fabricated modulator has an insertion loss of just 8 dB, which is in close agreement to simulation for a 500 µm-long device. Its voltage-length product was measured to be 4.2 Vmm by applying a DC bias. We attribute the difference between measured and simulated $V_\pi L$ to thin-film damage during a pre-fabrication substrate cleaning process, which can be easily rectified in future process runs, as well as the multi-domain nature of thin-film BTO [7].

3. Modulator Performance

Here we describe the modulator's performance in data transmission and long-term stability. Fig. 3(a) shows a schematic of the data transmission experiment. A tunable laser source (TLS) provided an optical carrier in the C-band that was amplified with an erbium-doped fiber amplifier (EDFA) before being coupled to and from the photonic integrated circuit through grating couplers. Electrical signals were generated with a 256 GSa/s arbitrary waveform generator (AWG) and amplified to a V_p of 2.8 V before being delivered to the modulator through RF probes in a push-pull configuration. No DC biasing was used during the experiments. At the receiver side, the modulated signal was amplified with an EDFA and sent to a photodetector (PD) for direct detection. A real-time 256 GSa/s digital sampling oscilloscope (DSO) captured the baseband signal from the PD and was saved for offline digital signal processing (DSP). The DSP consisted of matched filtering, timing recovery, T/2-spaced feed-forward equalization, pattern-based equalization, and T-spaced feed-forward equalization.

Eye diagrams of the received signals are shown in Fig. 3(b) for 128 GBd 2PAM and Fig. 3(c) for 100 GBd 4PAM. The 2PAM signal was received with a BER of 6.84×10^{-3} below the HD-FEC threshold with 8% overhead and an

SNR of 10.9 dB. The 4PAM signal was received with a BER of 3.89 × 10^{-2} below the SD-FEC threshold with 20% overhead and an SNR of 11.24 dB.

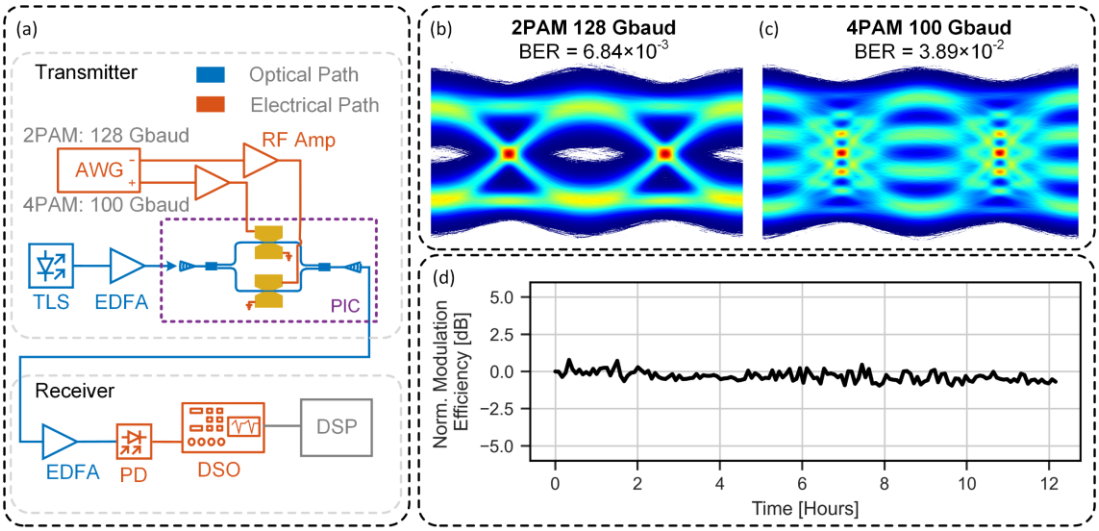

Fig. 3: (a) Schematic of the measurement setup. (b-c) Received eye diagrams after digital signal process for 128 GBaud 2PAM and 100 GBaud 4PAM. (d) Long-term stability measurement of continuous modulation with 20 dBm optical power.

The modulator also demonstrates excellent power handling capabilities. Fig. 3(d) shows the normalized modulation efficiency of the modulator over 12 hours while being continuously modulated with a single tone signal at 50 GHz and with an input optical power of 20 dBm. The flat modulation efficiency over the measurement time indicates no degradation of the modulator. The stability is a result of low ohmic losses in the weakly guided plasmonic structure and the robust nature of inorganic ferroelectric materials like BTO.

4. Summary

A weakly guided plasmonic modulator using BTO as the active material has been introduced. The modulator's structure combines the plasmonic benefits of using the electrodes for waveguiding with the photonic benefit of low insertion loss. The modulator demonstrates an insertion loss of 8 dB and a voltage-length product of 4.2 Vmm without the need for a DC bias during operation. Data transmission experiments show the ability to transmit 4PAM up to 100 GBaud for a maximum gross rate of 200 Gbit/s. The modulator additionally shows excellent stability at high optical powers with no degradation over 12 hours of continuous operation with 20 dBm of optical power. The weakly guided plasmonic BTO modulator shows potential for reducing the footprint of transmitters while keeping insertion losses low.

Acknowledgements

We wish to thank the Cleanroom Operations Team of the Binnig and Rohrer Nanotechnology Center (BRNC) for their help and support. This work was funded by the EC H2020 projects NEBULA (871658), PlasmoniAC (871391), and NEoteRIC (871330)

References

[1] P. J. Winzer and D. T. Neilson, 'From Scaling Disparities to Integrated Parallelism: A Decathlon for a Decade', *Journal of Lightwave Technology*, vol. 35, no. 5, pp. 1099–1115, Mar. 2017, doi: 10.1109/JLT.2017.2662082.

[2] M. Nowell, 'Cisco VNIForecast Update 2019', 2019.

[3] A. Rahim *et al.*, 'Taking silicon photonics modulators to a higher performance level: state-of-the-art and a review of new technologies', *AP*, vol. 3, no. 2, p. 024003, Apr. 2021, doi: 10.1117/1.AP.3.2.024003.

[4] Q. Hu *et al.*, 'Ultrahigh-Net-Bitrate 363 Gbit/s PAM-8 and 279 Gbit/s Polybinary Optical Transmission Using Plasmonic Mach-Zehnder Modulator', *Journal of Lightwave Technology*, vol. 40, no. 10, pp. 3338–3346, May 2022, doi: 10.1109/JLT.2022.3172246.

[5] M. Xu *et al.*, 'Dual-polarization thin-film lithium niobate in-phase quadrature modulators for terabit-per-second transmission', *Optica, OPTICA*, vol. 9, no. 1, pp. 61–62, Jan. 2022, doi: 10.1364/OPTICA.449691.

[6] S. Abel *et al.*, 'Large Pockels effect in micro- and nanostructured barium titanate integrated on silicon', *Nat. Mater.*, vol. 18, no. 1, Art. no. 1, Jan. 2019, doi: 10.1038/s41563-018-0208-0.

[7] A. Messner *et al.*, 'Plasmonic Ferroelectric Modulators', *Journal of Lightwave Technology*, vol. 37, no. 2, pp. 281–290, Jan. 2019, doi: 10.1109/JLT.2018.2881332.

[8] M. Kohli, D. Chelladurai, and J. Leuthold, '216 GBd Plasmonic Ferroelectric Modulator Monolithically Integrated on SIlicon Nitride', presented at the European Conference on Optical Communications, 2022.

[9] L. Lafone, T. P. H. Sidiropoulos, and R. F. Oulton, 'Silicon-based metal-loaded plasmonic waveguides for low-loss nanofocusing', *Opt. Lett., OL*, vol. 39, no. 15, pp. 4356–4359, Aug. 2014, doi: 10.1364/OL.39.004356.

[10] M. Zgonik *et al.*, 'Dielectric, elastic, piezoelectric, electro-optic, and elasto-optic tensors of ${\mathrm{BaTiO}}_{3}$ crystals', *Phys. Rev. B*, vol. 50, no. 9, pp. 5941–5949, Sep. 1994, doi: 10.1103/PhysRevB.50.5941.

[11] F. Eltes *et al.*, 'Low-Loss BaTiO3–Si Waveguides for Nonlinear Integrated Photonics', *ACS Photonics*, vol. 3, no. 9, pp. 1698–1703, Sep. 2016, doi: 10.1021/acsphotonics.6b00350.